GENERATION OF INTERNAL GRAVITY WAVES BY UNSTABLE OVERFLOWS

G. E. SWATERS
Department of Mathematical and Statistical Sciences, and
Institute of Geophysical Research
University of Alberta
Edmonton, AB, T6G 2G1 Canada

1. Introduction

The deep western undercurrent (DWUC) in the Atlantic ocean has, as one of its sources, the Denmark Strait Overflow (DSO). The DSO is an example of a sill-controlled abyssal gravity current. Greatly simplified, overflows of this kind initially exhibit pronounced down slope motion which subsequently evolves into more or less along slope motion, which is banked against sloping topography. This picture is, of course, far from complete. Baroclinic interactions with the overlying water column and non-conservative processes such as entrainment and friction are present. In addition, there is considerable spatial and temporal variability associated with these flows in both the near-sill and down stream regions.

Bruce (1995), examining satellite imagery, and Krause (1996), examining buoy trajectories, showed the development of down stream cyclonic eddies associated with the DSO. Recently analyzed observations and numerical simulations (Krauss and Käse, 1998; Käse and Oschlies, 2000; Girton and Sanford, 2001, 2002; Käse *et al.*, 2002) suggest that key aspects of the down stream mesoscale variability can be understood in the context of the (non-quasigeostrophic) baroclinic instability mechanism described by Swaters (1991) for abyssal currents, interpreted, of course, in the context of realistic physical oceanographic properties (e.g., Jiang and Garwood, 1996; Jungclaus *et al.*, 2001).

Käse *et al.* (2002), analyzing oceanographic data for the DSO region, from four different cruises over a three year period, and examining high resolution numerical simulations, describe the differing dynamical regimes between the near-sill and down stream overflow. In contrast to the down

stream flow, the near-sill overflow is predominately down slope, strongly influenced by bottom friction and is near, and even possibly super, critical (with respect to long internal gravity waves). Girton and Sanford (2002), using estimates derived from the aforementioned cruise data, argue, perhaps not surprisingly, that the near-sill momentum balance for the overflow is principally between rotation, down slope gravitational acceleration and bottom friction.

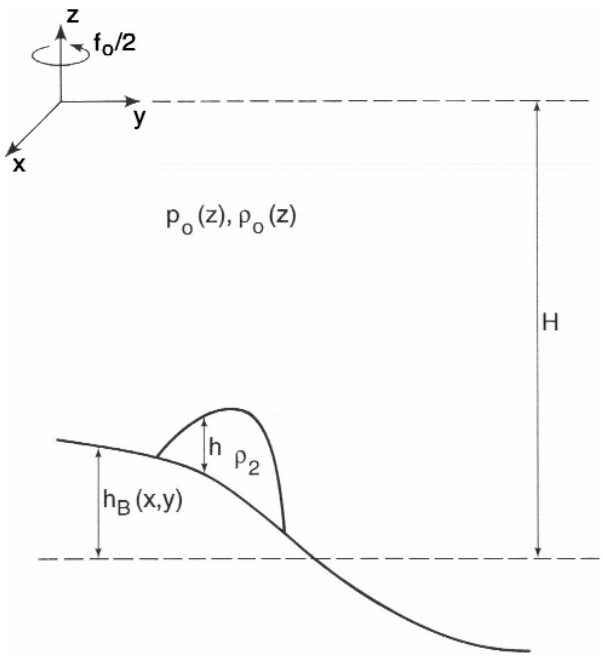

Fig. 1. Geometry of the model used in this paper.

These dynamical balances suggest another source for overflow variability, particularly in the near-sill region, and one which has not been explored before in this context. Frictional down slope flows which are super critical can be unstable. In the absence of rotation and baroclinicity, the instabilities are classical roll waves (Jeffreys, 1925; Whitham, 1974). For oceanographically relevant scales, the instabilities will, as we show, manifest themselves in the overlying ocean as amplifying long internal gravity waves. Within the overflow itself, the instabilities take the form of down slope propagating, growing periodic bores or pulses.

A summary is presented here of a simple theory for the frictional destabilization of abyssal overflows, with rotation and baroclinicity present, and of the characteristics of the internal gravity field, in the overlying ocean, associated with the instability. Full details can be found in Swaters (2003).

2. Model Equations

The underlying geometry is sketched in Fig. 1. We assume $f-$plane dynamics for a stably and continuously stratified fluid of finite depth overlying a well mixed abyssal current layer with variable bottom topography. The upper, i.e., the continuously stratified, layer is denoted as layer one. The abyssal current, i.e., the lower layer, is denoted as layer two. The upper and abyssal layer dynamical quantities will be denoted, unless otherwise specified, with a 1 and 2 subscript, respectively.

The theoretical model is based on the incompressible adiabatic equations under a Boussinesq approximation for a continuously stratified fluid for the upper layer and the shallow water equations for the abyssal layer. We assume a rigid ocean surface which will filter out the external gravity wave modes in the model and focus attention on the baroclinic aspects of the dynamics.

Assuming that $O\left(h/H\right)$ is small, the *nondimensional* model can be written in the form (see Swaters, 2003 for full details)

$$\left(\partial_{tt}+f^2\right)\left(B^{-1}\varphi_{zt}\right)_z+\triangle\varphi_t=0, \tag{1}$$

subject to

$$\varphi_{zt}=0 \text{ on } z=0, \text{ and } \varphi_{zt}=-B\left(-1\right)h_t \text{ on } z=-1, \tag{2}$$

with the auxiliary upper layer relations

$$\left(\partial_{tt}+f^2\right)\mathbf{u}_1=f\mathbf{e}_3\times\nabla\varphi-\nabla\varphi_t,\ \rho=-\varphi_z,\ w=-B^{-1}\varphi_{zt}, \tag{3}$$

where $h\left(x,y,t\right)$ is determined from the abyssal layer equations

$$\left(\partial_t+\mathbf{u}_2\cdot\nabla\right)\mathbf{u}_2+f\mathbf{e}_3\times\mathbf{u}_2=-\nabla\left(h+h_B\right)+\frac{1}{R_e}\frac{\nabla\cdot\left(h\nabla\mathbf{u}_2\right)}{h}-\frac{c_D\left|\mathbf{u}_2\right|\mathbf{u}_2}{h}, \tag{4}$$

$$h_t+\nabla\cdot\left(\mathbf{u}_2h\right)=0, \tag{5}$$

where the abyssal layer's Reynolds number, R_e, nondimensional Coriolis parameter (or, equivalently, the reciprocal of the temporal Rossby number), f, scaled bottom drag coefficient (or, equivalently, the reciprocal of the nonrotating Froude number), c_D, and the Burger number, $B\left(z\right)$, are given by, respectively,

$$f=\frac{f^*\sqrt{h_*/g'}}{s^*},\ B\left(z\right)=\frac{s^*N^2\left(Hz\right)H^2}{g'h_*},\ R_e=\frac{h_*\sqrt{g'h_*}}{A_Hs^*},\ c_D=\frac{c_D^*}{s^*},$$

where c_D^*, f^*, h_*, A_H, s^* are the bottom friction coefficient, local Coriolis parameter, scale abyssal layer thickness, horizontal eddy coefficient and

scale bottom slope parameter, respectively. The Brunt-Väisälä frequency, $N(z)$, and the reduced gravity, g', are given by

$$N^2(z) = -\frac{g}{\rho_2}\frac{d\rho_0(z)}{dz} > 0, \quad g' = \frac{g(\rho_2 - \rho_0(-H))}{\rho_2} > 0,$$

respectively where $\rho_0(z)$ and ρ_2 are the upper layer hydrostatic background and abyssal layer density, respectively. These equations remain valid in both the nonrotating $f = 0$ and inviscid $c_D = A_H = 0$ ($R_e \to \infty$) limits.

3. Normal Mode Stability Equations

We examine steady "slab" solutions (see, e.g., Jeffreys, 1925; Whitham, 1974; Baines, 1995) given by

$$\mathbf{u_2} = (U, V), \quad h = 1, \tag{6}$$

for the linearly sloping bottom $h_B = -y$. These uniform flows are equivalent to the solutions found for "stream tube" models, without along-stream variation, which have been used to examine aspects of the dynamics of rotating turbidity and abyssal currents (e.g., Smith, 1975; Killworth, 1977; Price and Baringer, 1994; Emms, 1998).

Substitution of (6) into (4) yields (continuity is trivially satisfied)

$$fV = c_D\left(U^2 + V^2\right)^{\frac{1}{2}} U, \tag{7}$$

$$fU = 1 - c_D\left(U^2 + V^2\right)^{\frac{1}{2}} V, \tag{8}$$

which can be solved to give

$$(U, V) = \left(f\gamma^2, c_D\gamma^3\right); \gamma \equiv \sqrt{\frac{2}{f^2 + \sqrt{f^4 + 4c_D^2}}} > 0. \tag{9}$$

Fig. 2 is a stick plot of the steady uniform velocity (U, V), determined by (7) and (8), as a function of the bottom friction coefficient c_D and the nondimensional Coriolis parameter f for the range $0.1 \leq c_D \leq 0.5$ and $0.1 \leq f \leq 1.0$. In order to ensure that the vectors remain within the plot boundaries, the velocity vectors have been scaled so that the maximum speed, which occurs for the velocity vector located at $c_D = f = 0.1$ in Fig. 2 (the velocity vector located at the lower left hand corner), has length 0.2. In addition, the vectors are oriented so that down slope motion is indicated by the vector pointing in the direction of increasing f. Rightward deflected (which occurs for positive f) along slope motion is indicated by the vector

pointing in the direction of increasing c_D. The orientation is shown in the lower right corner in Fig. 2 by a (U, V) coordinate axes. We see the general trend from down (along) slope motion to along (down) slope motion as f (c_D) increases for a given c_D (f), within the context that the speed monotonically decreases as c_D and f individually increase.

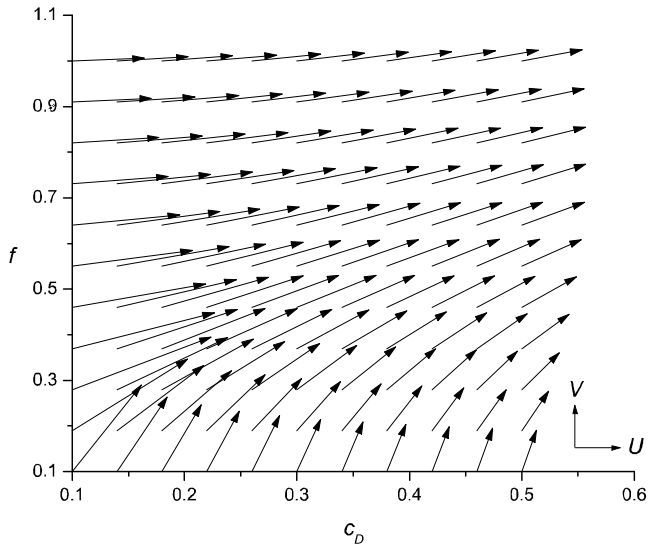

Fig. 2. $(U,\ V)$ in the $(c_D,\ f)-$plane.

The general normal mode stability problem is determined by substituting

$$(u, v, h) = (U, V, 1) + \left(\widetilde{u}, \widetilde{v}, \widetilde{h}\right) \exp\left[ikx + ily + (\sigma - ikU - ilV)\, t\right] + c.c., \tag{10}$$

$$\varphi = \psi\,(z) \exp\left[ikx + ily + (\sigma - ikU - ilV)\, t\right] + c.c., \tag{11}$$

into (1), (2), (4) and (5), giving

$$\psi_{zz} - \lambda^2 \psi = 0;\ \lambda^2 \equiv \frac{\left(k^2 + l^2\right) B}{(\sigma - ikU - ilV)^2 + f^2}, \tag{12}$$

subject to

$$\psi_z = 0 \text{ on } z = 0, \text{ and } \psi_z = -Bh \text{ on } z = -1, \tag{13}$$

with

$$\mathcal{M}\left[u, v, h\right]^\top = \mathbf{0}, \tag{14}$$

where we have assumed, for convenience, a constant Burger number, dropped the tildes, and where $\mathcal{M}$ is the 3×3 matrix

$$\begin{bmatrix} \sigma + \frac{k^2+l^2}{R_e} + c_D\gamma\left(1+\gamma^2 f^2\right) & f\left(c_D^2\gamma^4 - 1\right) & ik - c_D f\gamma^3 \\ f\left(1+c_D^2\gamma^4\right) & \sigma + \frac{k^2+l^2}{R_e} + c_D\gamma\left(1+c_D^2\gamma^4\right) & il - c_D^2\gamma^4 \\ ik & il & \sigma \end{bmatrix}. \tag{15}$$

The vertical structure of the normal modes in the upper layer is determined by the solution to (12) and (13), and is given by

$$\psi(z) = \frac{Bh\cosh(\lambda z)}{\lambda\sinh(\lambda)}, \tag{16}$$

which implies that the vertical structure in the (normal mode) vertical velocity will be described by

$$\widetilde{w}(z) = \frac{(ikU + ilV - \sigma)}{B}\psi_z = \frac{(ikU + ilV - \sigma)\, h\sinh(\lambda z)}{\sinh(\lambda)}. \tag{17}$$

Equation (14) has nontrivial solutions if and only if

$$\det \mathcal{M} = 0, \tag{18}$$

which gives rise to a cubic polynomial in σ which can be solved to give solutions of the form

$$\sigma = \sigma\left(c_D,\ f,\ R_e,\ k,\ l\right). \tag{19}$$

Instability occurs if the growth rate $\mathrm{Re}(\sigma) > 0$.

In the non-rotating limit it can be shown (Swaters, 2003) that (18) reduces, for the non-trivial modes, to

$$\sigma = -\left(\sqrt{c_D} + \frac{l^2}{2R_e}\right) \pm \sqrt{\left(\sqrt{c_D} + \frac{l^2}{2R_e}\right)^2 - (il + l^2)}, \tag{20}$$

where we have assumed $k = 0$. A mode for a given l will be stable provided

$$\mathrm{Re}\left\{\sqrt{\left(\sqrt{c_D} + \frac{l^2}{2R_e}\right)^2 - (il + l^2)}\right\} \leq \sqrt{c_D} + \frac{l^2}{2R_e},$$

which is satisfied *if and only if* $\sqrt{c_D} + l^2/(2R_e) \geq 1/2$. Thus, in the non-rotating limit, $c_D \geq \frac{1}{4} \Longleftrightarrow$ stability which is just the classical roll wave stability result (see, e.g., Jeffreys, 1925; Whitham, 1974; Baines, 1995).

4. Stability Characteristics

Fig. 3 is a contour plot of the growth rate of the most unstable mode (denoted as $\mathrm{Re}\,(\sigma_{\max})$) in the $(c_D,\ f)-$ plane assuming $R_e = 400.0$. The most unstable mode, denoted as $\sigma_{\max}$, is that normal mode with the largest value of $\mathrm{Re}\,(\sigma)$ considered as a function of the wave numbers (k, l) for a given value of the parameters $(c_D,\ f,\ R_e)$. We denote the wave number of the most unstable mode by $(k_{\max},\ l_{\max})$.

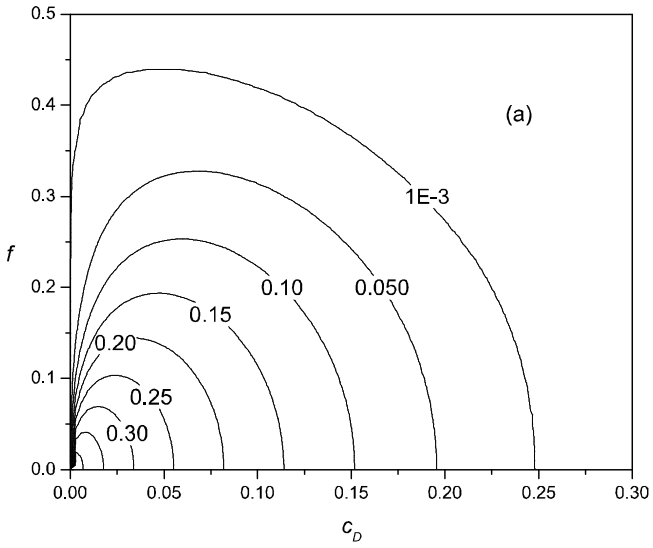

Fig. 3. $\mathrm{Re}\,(\sigma_{\max})$ in the $(c_D,\ f)-$ plane.

In Fig. 3 we can see that the sharp cutoff value for instability associated with the bottom friction coefficient continues to exist (but decreases) as f increases from zero. Instability continues to occur for $f > 0$, but does so for a smaller range of c_D values. In the non-rotating limit, the bottom friction coefficient cutoff value is given exactly by $c_D = 0.25$.

Although it is difficult to discern clearly in Fig. 3, there is a sharp boundary with respect to f, i.e., there is a distinct marginal stability curve, between the region of instability (where the growth rate is positive) and the region of stability (where the most unstable mode has zero growth rate, i.e., the abyssal flow is neutrally stable). The contour labelled 0.001 is very close to this boundary. (When we tried to contour the $0-$growth rate isoline exactly the contour package introduced a highly irregular multiply connected pattern.)

As f increases, Fig. 3 shows that the growth rate of the most unstable mode decreases monotonically. Nevertheless, Fig. 3 suggests that the frictional destabilization of abyssal overflows is possible for physically realizable values of f or, equivalently, the inverse Rossby number. For example, for $c_D = 0.1$ and $f = 0.25$ (i.e., a Rossby number of about 4.0), the most unstable mode has a (nondimensional) growth rate of about 0.09 which corresponds to a (dimensional) $e-$ folding time of about 24 hours (the time scale is about 2.2 *hours*). For $c_D = 0.1$ and $f = 0.25$, $U = 1.84$ and $V = 1.99$ which imply a *dimensional* along and cross slope velocity for the mean overflow of about 110 cm/s and 120 cm/s, respectively (the abyssal velocity scale is about 60 cm/s).

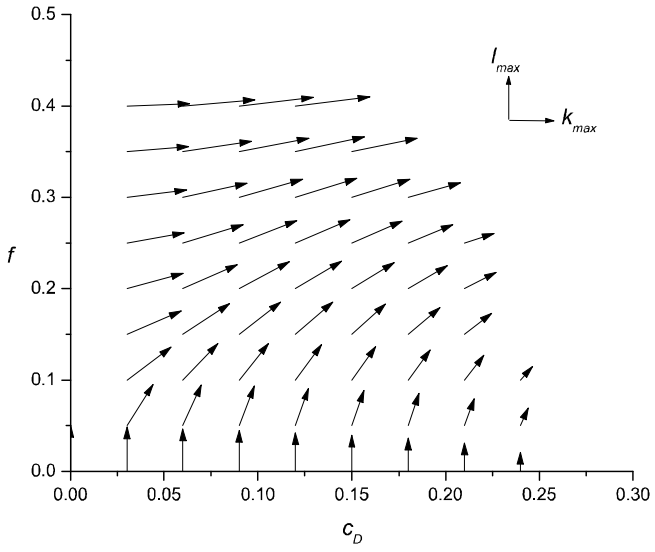

Fig. 4. $(k_{\max},\ l_{\max})$ in the $(c_D,\ f)-$plane.

Fig. 4 is a stick plot of the wave number vector $(k_{\max},\ l_{\max})$ as a function of the bottom friction coefficient c_D and the nondimensional Coriolis parameter f for the range $0 \leq c_D \leq 0.3$ and $0 \leq f \leq 0.5$. In order to ensure that the vectors remain within the plot boundaries, the velocity vectors have been scaled so that the length of the wave number vector located at $c_D = f = 0$ in Fig. 4 (located at the lower left hand corner), has length 0.05 (its actual length is about 2.58).

The wave number vectors are oriented so that positive $l_{\max}$ is indicated by the vector pointing in the direction of increasing f. Positive $k_{\max}$ is indicated by the vector pointing in the direction of increasing c_D. The orientation is shown in the upper right corner in Fig. 4 by a $(k_{\max},\ l_{\max})$

coordinate axes. The region of stability in the $(c_D,\ f)-$ plane has no wave number vector shown because $(k_{\max},\ l_{\max}) = \mathbf{0}$ there. The reason that *both* $l_{\max}$ and $k_{\max}$ will be zero in the region of stability, away from the marginal stability boundary, is a consequence of the presence of horizontal friction in the linear stability problem. The *most unstable mode* in the region of stability, when horizontal friction is present (which is proportional to the Laplacian operator), occurs when the magnitude of the wave number vector is zero since any other wave number pair will necessarily result in a more negative growth rate, when all other parameters are held constant. One can also see the general trend for the increasing orientation toward along slope propagation as f increases for a given c_D. In addition, one can see the general trend of diminishing $k_{\max}$ as c_D increases for a given f as well as an overall decrease in the magnitude of the wave number vector (i.e., a trend to longer waves).

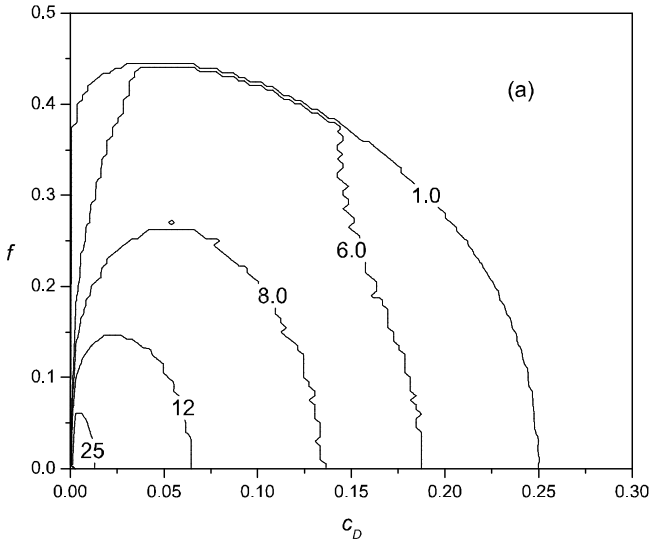

Fig. 5. $\omega_{\max}^{geo}$ in the $(c_D,\ f)-$ plane.

It is useful to give a dimensional estimate of $(k_{\max}, l_{\max})$. If we consider $c_D = 0.1$ and $f = 0.25$, we find that $k_{\max} \approx 1.55$ and $l_{\max} \approx 1.29$, which implies a *dimensional* along slope wave length of about 20 km and a cross slope wave length of about 24 km for a total wave length of about 31 km for the most unstable mode associated with $c_D = 0.1$ and $f = 0.25$ (the length scale is about 5 km).

Fig. 5 is a contour plot of the *geostationary* frequency of the most unstable mode, given by

$$\omega_{\max}^{geo} = Uk_{\max} + Vl_{\max} - \mathrm{Im}\left(\sigma_{\max}\right),$$

in the $(c_D,\ f)-$ plane for $R_e = 400.0$. The geostationary frequency is the frequency one would measure using bottom moored instruments. As f increases, away from $c_D = 0$ (the $f-$axis), we see the general trend to lower, yet not sub-inertial, frequencies. If we consider $c_D = 0.1$ and $f = 0.25$, we find that $\omega_{\max}^{geo} \approx 7.45$, which implies a *dimensional geostationary* period of about 2 *hours*.

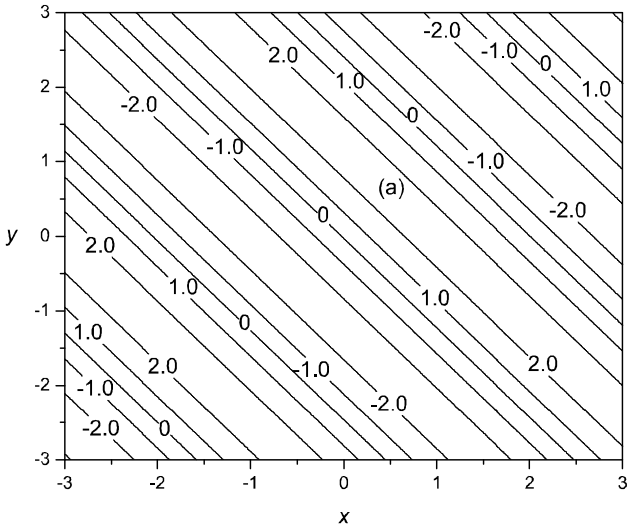

Fig. 6. $w\left(x,\ y,\ -1,\ 0\right)$ in the $(x,\ y)-$plane.

Fig. 6 is a contour plot of a horizontal section of the *total* vertical velocity in the overlying ocean, given by,

$$w\left(x,y,z,t\right) = \mathrm{Re}\left\{\widetilde{w}\left(z\right)\exp\left[ikx + ily + \left(\sigma - ikU - ilV\right)t\right]\right\},$$

for $z = -1$ (immediately above the abyssal overflow), $t = 0$, $B = 1$ and $h = 1$ (for convenience) for the most unstable mode

$$\sigma_{\max} \approx 0.09 - 2.04i,\ k_{\max} \approx 1.55,\ l_{\max} \approx 1.29,$$

$$U \approx 1.84,\ V \approx 1.99,$$

for $c_D = 0.1$ and $f = 0.25$. We recall that the bottom topography is given by $h_B = -y$ so that the depth increases with increasing y. The wave field propagates from the lower left corner toward the upper right corner.

The upper layer vertical velocity scale is about 1.2 cm/s. Thus, assuming a *nondimensional* perturbation thickness in the abyssal current of about 0.1 (corresponding to about a *dimensional* abyssal current height anomaly of about 10 m), Fig. 6 suggests a *dimensional* vertical velocity in the overlying water column, immediately above the abyssal current, associated with the generated internal gravity wave field of about 0.25 cm/s. We note again that Fig. 6 assumes that $h = 1$, so that $h = 0.1$ would reduce the w values by a factor of 10.

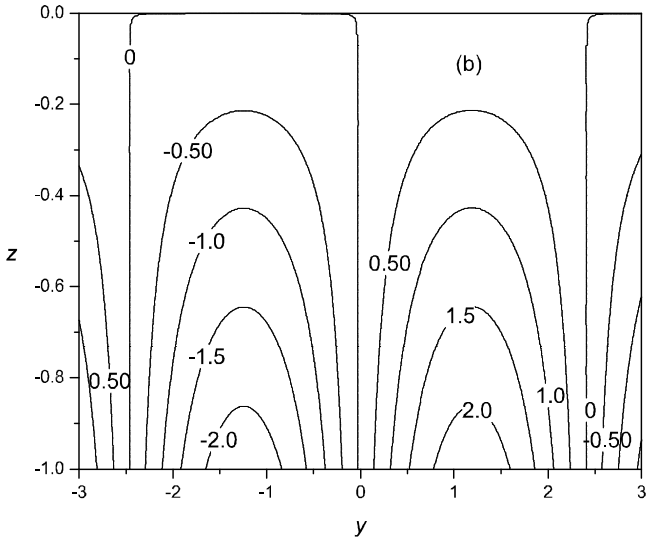

Fig. 7. $w\,(0,\ y,\ z,\ 0)$ in the $(y,\ z) -$ plane.

Fig. 7 is a contour plot of a vertical section of the *total* vertical velocity in the overlying ocean along $y = 0$ with $t = 0$ and $h = 1$ (again, for convenience) for the most unstable mode for $c_D = 0.1$ and $f = 0.25$. One can see the bottom intensification in the internal wave field and, for $B = 1$, the approximate linear decrease in the magnitude of w with decreasing depth. For larger values of B, the internal gravity wave field is increasingly bottom intensified.

Acknowledgments

Preparation of this manuscript was supported in part by Research Grants awarded by the Natural Sciences and Engineering Research Council (NSERC) of Canada. Email: gordon.swaters@ualberta.ca.
URL: pacific.math.ualberta.ca/gordon.

References

Baines, P. G., 1995: *Topographic Effects in Stratified Flows.* Cambridge University Press, 482 pp.

Bruce, J. G., 1995: Eddies southwest of Denmark Strait. *Deep-Sea Res.,* **42**, 13-29.

Emms, P. W., 1998: A streamtube model of rotating turbidity currents. *J. Mar. Res.,* **56**, 41-74.

Girton, J. B., and T. B. Sanford, 2001: Synoptic sections of the Denmark Strait overflow. *Geophys. Res. Lett.* **28**, 1619-1622.

Girton, J. B., and T. B. Sanford, 2002: Descent and modification of the Denmark Strait overflow. Submitted to *J. Phys. Oceanogr.*

Jeffreys, H., 1925: The flow of water in an inclined channel of rectangular bottom. *Phil. Mag.*, **49**, 793-807.

Jiang, L., and R. W. Garwood, 1996: Three-dimensional simulations of overflows on continental slopes. *J. Phys. Oceanogr.,* **26**, 1214-1233.

Jungclaus, J. H., J. Hauser, and R. H. Käse, 2001: Cyclogenesis in the Denmark Strait Overflow plume. *J. Phys. Oceanogr.,* **31**, 3214-3228.

Käse, R. H., Girton, J. B., and T. B. Sanford, 2002: Structure and variability of the Denmark Strait overflow: Model and observations. Submitted to *J. Geophys. Res.*

Käse, R. H., and A. Oschlies, 2000: Flow through Denmark Strait. *J. Geophys. Res.*, **105**, 28527-28546.

Krauss, W., 1996: A note on overflow eddies. *Deep-Sea Res.,* **43**, 1661-1667.

Killworth, P. D., 1977: Mixing on the Weddell Sea continental slope. *Deep-Sea Res.,* **24**, 427-448.

Krauss, W., and R. H. Käse, 1998: Eddy formation in the Denmark Strait overflow. *J. Geophys. Res.*, **103**, 15523-15538.

Price, J. F., and M. O. Baringer, 1994: Outflows and deep water production by marginal seas. *Progr. Oceanogr.*, **33**, 161-200.

Smith, P. C., 1975: A streamtube model for bottom boundary currents in the ocean. *Deep-Sea Res.,* **22**, 853-873.

Swaters, G. E., 1991: On the baroclinic instability of cold-core coupled density fronts on a sloping continental shelf. *J. Fluid Mech.*, **224**, 361-382.

Swaters, G. E., 2003: Baroclinic characteristics of frictionally destabilized abyssal overflows. Submitted to *J. Phys. Oceanogr.*

Whitham, G. B., 1974: *Linear and Nonlinear Waves.* Wiley, 636 pp.